

1 **This manuscript has been submitted for publication to *Seismological Research***  
2 **Letters. Please note that, despite undergoing peer-review, the manuscript has yet**  
3 **to be accepted for publication. Subsequent versions of this manuscript may have**  
4 **slightly different content. If accepted, the final version of this manuscript will be**  
5 **available via the '*Peer-reviewed Publication DOI*' link on the right-hand side of this**  
6 **webpage. Please feel free to contact any of the authors; we welcome feedback.**

7  
8 **Title**

9 Evaluation of the Grillo sensor, a low-cost accelerometer for IoT-based Real-time  
10 seismology

11  
12 **Authors**

13 Vaclav Kuna<sup>1</sup>, Diego Melgar<sup>2</sup>, Andres Meira<sup>3</sup>

14 **Author affiliation**

15 1. The Institute of Geophysics of the Czech Academy of Sciences, Prague, Czech  
16 Republic

17 2. Department of Earth Sciences, University of Oregon, Eugene, Oregon, United States

18 3. Grillo Holdings Inc., Cazenovia, NY, USA

19 **Abstract**

20 Micro-Electro-Mechanical (MEMS) accelerometers are useful for real-time seismology  
21 due to their ability to record strong, unsaturated seismic signals. Recent advances in  
22 MEMS technologies enable design of instruments with improved capabilities that also  
23 allow recording of small signals. As a result, MEMS can be useful across a broad  
24 dynamic range and for both major earthquakes and smaller magnitude events.  
25 Leveraging improved capabilities from off-the-shelf components, we demonstrate a  
26 new, low-cost MEMS-based accelerometer that provides an optimal tradeoff between  
27 instrument cost and performance. This article analyzes the instrument's performance in  
28 a regional network deployed in southern Mexico over a period of 3+ years for the  
29 purpose of earthquake early warning. We discuss the self-noise level, dynamic range,  
30 and useful resolution, and compare these parameters to other MEMS-based  
31 instruments. Besides the sensor evaluation, we present a large, openly available  
32 dataset of strong motion data that comprises continuous ground motion records from 24  
33 instruments since 2017.

34

35

36 **Introduction**

37 Many regions of the world suffer from high earthquake-related risks due to a  
38 combination of growing population in hazard prone areas and fragile infrastructure that  
39 might not withstand strong ground shaking (Silva *et al.*, 2018). Earthquake Early

40 Warning (EEW) systems can reduce these risks by providing users a short time window  
41 for taking a basic protective action before the strong shaking arrives. EEWs have  
42 proven to be capable of providing timely alerts during earthquakes in Mexico (Aranda *et*  
43 *al.*, 1995), Japan (Wenzel and Zschau, 2014), and Taiwan (Chen *et al.*, 2015). Multiple  
44 other EEW systems are either in development or undergoing testing (Allen and Melgar,  
45 2019), such as on the US West coast (Kohler *et al.*, 2018), in Italy (Satriano *et al.*,  
46 2011), and in China (Jin *et al.*, 2013).

47 There are two basic approaches to EEW systems. Regional or network-based EEW's  
48 make use of seismic networks located in, or near, a well-known seismic zone and aim to  
49 detect and characterize earthquakes a few seconds after their origin. Such systems  
50 exploit the difference between the fast electromagnetic communication of the system  
51 and the slower speed of seismic waves. Regional EEW's can provide useful alerts to  
52 sites farther than about 50 km from the earthquake epicenter. In contrast, on-site or  
53 single-station EEW's use the initial portion of the P-wave to predict the peak ground  
54 acceleration (often associated with slower S-wave) at that same site and are suitable for  
55 locations closer to the earthquake epicenter. Invariably, the choice of the type of system  
56 and algorithm depends strongly on available budgets. Sensor networks, including  
57 material cost and sensor deployment are one of the largest expenses in an EEW  
58 system and so the design of the system will be strongly controlled by how many stations  
59 can be afforded and what size area the system needs to serve with that limited budget.  
60 For this reason, a low cost sensor that can be deployed in large numbers to provide  
61 dense station coverage across a large area has always been desirable.

62 Micro-electro-mechanical systems (MEMS) capacitive accelerometers offer this  
63 capability. They are low-cost, low-power sensors with a wide range of applications in  
64 multiple fields, such as electronics, engineering, and the military. Seismic applications  
65 have utilized MEMS sensors since the early 2000s (Holland, 2003). Their ability to  
66 record unsaturated, high-frequency, and especially near-field ground-motions (Evans et  
67 al., 2014), make them an economical choice for large-scale or dense seismic networks  
68 appropriate for EEW systems. MEMS instruments have been proven to be effective for  
69 regional EEW systems (Wu, 2015; Wu *et al.*, 2016; Peng *et al.*, 2019), on-site EEWs  
70 (Wu *et al.*, 2013, 2016), or used to densify existing networks of traditional, force-balance  
71 seismometers (Nof *et al.*, 2019). Kong *et al.* (2016) also designed a decentralized EEW  
72 based on crowdsourcing acceleration data from smartphone MEMS and Cochran *et al.*  
73 (2009) demonstrated using MEMS sensors in personal laptops.

74 In the past decade, scientists and engineers developed several MEMS-based  
75 instruments for EEW utilizing low-cost off-the-shelf components. Instruments such as  
76 Palert (Wu *et al.*, 2013), EDAS-MAS (Peng *et al.*, 2013), and Onavi (Cochran *et al.*,  
77 2009) proved to be useful for recording high-amplitude ground motion. However, these  
78 kinds of sensors have relatively high self-noise, low resolution, and dynamic range, and  
79 as a result they fail to record small amplitude signals. Therefore, most of these rank  
80 among what is defined as a "Class-C" type instrument according to the Advanced  
81 National Seismic System (ANSS) categorization (USGS Open-File Report 2008-1262;  
82 Evans et al., 2014). This is a commonly accepted set of standards which classifies  
83 strong motion instruments based on their resolution and dynamic range. Other  
84 instruments, such as MAMA (Nof *et al.*, 2019), SOSEWIN (Fleming *et al.*, 2009), or GL-

85 P2B (Peng *et al.*, 2017, 2019), have incorporated multiple analog MEMS sensors into a  
86 single device. In doing so, these instruments show improved data quality, allowing some  
87 of them to be ranked as ANSS Class B; however, the greater complexity of these  
88 devices results in increased manufacturing costs.

89 MEMS technologies have continued to evolve and more recent advances have  
90 improved the quality of off-the-shelf components to the point that they now offer reduced  
91 self-noise and higher resolution than their ancestors. To leverage the capabilities of  
92 present-day components and maximize the performance of off-the-shelf MEMS  
93 sensors, Grillo, a social enterprise startup based in Mexico, has developed a new  
94 seismic instrument for EEW and other real-time seismology applications. The total cost  
95 of the instrument that features a high-resolution, low-noise, low-power MEMS sensor is  
96 less than 100 USD.

97 The development of the new instrument is a part of a broader effort of developing a  
98 lightweight, low-cost EEW system based on the concept of the Internet of Things (IoT),  
99 that is, a system of mutually connected sensors and devices that exchange data over  
100 the internet. Using the IoT infrastructure, the Grillo instruments transmit real-time  
101 ground motion observations from sensors to cloud servers for detection, signal  
102 processing, and alert generation. Grillo has been testing the system in Mexico since  
103 2017, where a seismic network located at the southeast coast of the country provides  
104 earthquake alerts to users in densely populated regions inland.

105 This article describes the design of the instrument and evaluates the sensor's  
106 performance in terms of self-noise, dynamic range, and useful resolution. We focus on

107 both small amplitude signals such as P-waves as well as large amplitude ground  
108 motions. We discuss the sensor's reliability and compare its performance to other  
109 MEMS-based sensors developed for EEW applications. Finally, we also present a  
110 strong motion dataset collected during the 3-year deployment of 24 Grillo stations in a  
111 highly seismically active region in Mexico. We analyze signals of more than 700  
112 earthquakes recorded at the network (including two major  $M_w > 7$  events) and show  
113 that the Grillo instruments can, indeed, provide reliable information for rapid  
114 characterization of the earthquake source.

115

### 116 **The Grillo seismic sensor**

117 The sensor was designed with the primary goal of creating a reliable, high-performance,  
118 low-cost strong-motion sensor. The instrument consists of two major hardware  
119 components - the MEMS accelerometer module and the CPU module with Wifi and  
120 ethernet radios for data transmission.

121 The instrument uses the ADXL355 triaxial, low-noise, low-power MEMS accelerometer,  
122 with the selectable full-scale range of  $\pm 2, 4, \text{ or } 8 \text{ g}$  and an in-built 20-bit analog-to-digital  
123 (AD) converter. For the  $\pm 2 \text{ g}$  option selected for the Grillo instrument, the sensor offers a  
124 resolution of  $\sim 4 \mu\text{g}/\sqrt{\text{Hz}}$ , which is roughly 1/5 of the sensor noise density of  $22.5 \mu\text{g}/\sqrt{\text{Hz}}$   
125 in the bandwidth of 0.095-1000 Hz (URL for the complete sensor specifications can be  
126 found in Data and Resources section). The sensor sampling rate can be configured to  
127 31.25 or 125 Hz.

128 The Grillo instrument uses a Raspberry Pi 3b, this is a single-board computer with a 1.2  
129 GHz 64-bit quad-core processor, with integrated Wi-Fi, Bluetooth, and Ethernet  
130 connectivity.

131

### 132 **Grillo network and dataset**

133 In late 2017, Grillo installed a network of 24 instruments along the Pacific coast in  
134 southwest Mexico to test the new strong-motion instrument and the overall feasibility of  
135 the IoT-based EEW system. This region of the country is highly seismically active due  
136 to the ongoing subduction of the Cocos plate underneath the North American Plate.  
137 This generated more than two dozen earthquakes larger than Mw 7.0 in the past 50  
138 years (<http://www.ssn.unam.mx/>). The most destructive earthquake in modern times  
139 was the Mw 8.1 September 19, 1985, Michoacan event (Singh et al., 1988). Although  
140 350 km from the earthquake rupture zone, the earthquake caused extensive damage  
141 and more than 20,000 casualties in Mexico City due to its setting on lakebed sediments  
142 that amplified the seismic waves and resonated at frequencies destructive for mid-rise  
143 buildings (Campillo *et al.*, 1989).

144 The EEW network (Fig. 1) consists of coastal sites located near the subduction front. It  
145 was designed to provide earthquake early warnings for the densely populated regions  
146 further inland in central Mexico, including Mexico City. The instruments are placed in  
147 schools, hospitals, and government buildings in the states of Guerrero (16 instruments),  
148 Oaxaca (6), Chiapas (1), and in Mexico City (1) (Fig. 1a). Each sensor is mounted on a

149 primary structural element (e.g., concrete pillar) in the ground level of the building, with  
150 particular attention paid to searching for a quiet site. The sensors are leveled and  
151 connected by a power adapter and ethernet. They transmit live, 32 samples-per-second  
152 data streams to the Grillo platform on Amazon Web Services cloud via the MQTT  
153 protocol. Depending on the quality of internet connection, the data transmission latency  
154 is between 50 and 300 ms.

155 The network has recorded 722 events in the M 3.5-7.4 range (Fig. 1, 2) and the entire  
156 1.1 TB dataset is openly available (see Data and Resources for details). The median  
157 data return from all stations until November 2017 is 81% (Fig. 1c). Data gaps are  
158 caused primarily by power and connectivity issues. Due to the lack of instrument  
159 maintenance in 2019, the data recovery drops from ~70% in 2018 to 50% in 2019 and  
160 increases to ~90% in 2020.

161

## 162 **Sensor performance**

163 To evaluate the sensor's performance and its ability to record low-amplitude signals  
164 from small earthquakes, or large earthquakes occurring at a distance, we analyze the  
165 instrument's noise-level, dynamic range (DR), and useful resolution (NU).

166 We select 1-hour long instrument records (112500 samples) in three time periods in  
167 2018, 2019, and 2020. These periods are chosen to maximize the number of live  
168 instruments in the three calendar years - all 24 instruments were live on July 6, 2018,  
169 21:00-22:00, 19 on December 17, 2019, 17:00-18:00; and 18 on August 7, 2020, 1:00-



170 2:00. We filter the data with a 4-pole Butterworth high-pass filter with a corner frequency  
171 of 0.01 Hz and ensure that the records do not contain any transient signals. For each  
172 instrument, we calculate the root mean square (RMS) of the vertical (V) and two  
173 horizontal (H1, H2) instrument components (Table 1). The RMS values are significantly  
174 higher than the ambient noise levels suggesting that the collected data represent the  
175 sensor's self-noise.

176 The RMS values are almost identical for the sensor's V and H1 component, averaging  
177 about 42  $\mu\text{g}$ . The H2 component RMS is  $\sim 50\%$  higher, which is due to differences in the  
178 construction of the individual components of the triaxial MEMS sensor. V and H1 are  
179 determined from capacitance between a set of movable plates along the flat dimension  
180 of the sensor; the H2 is measured by a single capacitor plate fixed on the torsion spring.  
181 The mean RMS values did not change significantly throughout the deployment,  
182 demonstrating the performance stability and reliability of the sensor. Following the  
183 definitions in Peng *et al.* (2019), we calculate the DR and NU using the mean RMS  
184 values and the full-scale seismometer range of  $\pm 2$  g. For the V and H1 components, the  
185 DR averages over 90 dB; for H2, the DR is lower, with the mean value of 87 dB. The  
186 DR results in the useful resolution NU of 15 bits for V and H1 and 14.5 bits for H2.

187 We calculate the power spectral density (PSD) using the vertical components (Fig. 3).  
188 The PSD indicates an almost flat noise level of -77 dB (re 1  $\text{m/s}^2$ ) from 30 s to 10 Hz,  
189 with a gentle roll-off to -81 dB towards the Nyquist frequency (16 Hz). The PSD exceeds  
190 the microseismic high-noise model (HNM) in the entire frequency bandwidth, reaching  
191 roughly 20 dB higher than the HNM at the peak period of  $\sim 5$  s. Comparison with

192 representative earthquake spectral responses indicates that the sensor can detect peak  
193 accelerations of earthquakes with  $M > 2.5$ . at 10 km distance and  $M > 4.5$  at 100 km  
194 distance (Clinton and Heaton, 2002).

195 We also compare the sensor performance against other MEMS-based accelerometers  
196 (Fig. 3a). The self-noise level is 25-50 dB lower than the self-noise of Class C MEMS  
197 sensors commonly used in consumer devices, such as smartphones (Kong *et al.*,  
198 2016). It also performs better than instruments that use a single MEMS sensor, such as  
199 Onavi-B (Nof *et al.*, 2019). The performance of the Grillo instrument is similar to more  
200 complex MEMS-based accelerometers utilizing a series of sensors, such as MAMA (Nof  
201 *et al.*, 2019) and GL-P2B (Peng *et al.*, 2013). The sensor's overall performance,  
202 including the DR and the 20-bit AD converter resulting in the 4  $\mu\text{g}$  resolution, rank the  
203 Grillo instrument into Class B of ANSS strong motion sensor classification.

204

## 205 **Initial Observations and Results**

206 Over the 3-year observation period, the network has recorded more than a thousand  
207 earthquakes. To show the instrument's capability for reliable recording of signals with a  
208 wide range of amplitudes, we analyze earthquake P-waves obtained by manual picking  
209 using the Pyrocko toolbox (Heimann *et al.*, 2017). Our network captured 722  
210 earthquakes that allowed for reliable P-wave picking. For these events, we obtain  
211 earthquake source parameters (epicentral location, origin time, and magnitude) from the  
212 Mexican National Seismological Service (Servicio Sismológico Nacional; SSN)

213 earthquake catalog. The Grillo network recorded earthquakes in the magnitude range  
214 between 3.5 and 7.4, recording 187 earthquakes of  $M < 4$ ; 478 of  $4 < M < 5$ ; 43 of  $5 < M < 6$ ;  
215 2 of  $6 < M < 7$ ; 2 of  $M < 7$  (Fig. 1b). We were able to pick P-waves for  $M < 4$  earthquakes up  
216 to about 25 km away from the epicenter; the distance increases to 80 km for events  
217  $4 < M < 5$  and 150 km for  $5 < M < 6$ .

218 Earthquake magnitude in EEW is commonly estimated via the peak ground  
219 displacement ( $P_d$ ) of the initial portion of the earthquake's P-wave (Li *et al.*, 2017;  
220 Trugman *et al.*, 2019). The decadic logarithm of  $P_d$  increases linearly with earthquake  
221 magnitude up to a magnitude of saturation. The magnitude of saturation depends on the  
222 length of the P-wave segment used for the calculation and can reach up to  $M 7.5$  for  
223 roughly 10 s of initial P-wave (Trugman *et al.*, 2019). We calculated the  $P_d$  for 722  
224 earthquakes (Fig. 1) using records filtered by the 4-pole Butterworth bandpass filter  
225 between 0.075 and 3 Hz (as used e.g. Li *et al.*, 2017; Trugman *et al.*, 2019). We use 1,  
226 3, and 5 s long segments of the initial earthquake P-wave and correct the  $P_d$  to the  
227 common epicentral distance of 10 km. We observe a robust scaling of the  $P_d$  in the  
228 magnitude range between 3.5 and 6 for all lengths of the P-wave segments (Fig. 4).  
229 Earthquakes above this range also fit the predicted trend well. The  $P_d$  keeps increasing  
230 for earthquakes with  $M > 6$  (especially for the  $M 7.4$  La Crucecita earthquake) for all 1,  
231 3, and 5 s long time windows, with no obvious sign of saturation. However, given that  
232 the data set is sparse for large events (only two earthquakes with  $M > 6$ ), this result is  
233 not conclusive.

234 Two major earthquakes occurred during the period of observation. The first was the Mw  
235 7.2 Pinotepa earthquake (UNAM Seismology Group, 2013, Li et al., 2018), which  
236 impacted the southwest coast of Oaxaca State on February 16, 2018. Maximum  
237 observed shaking intensities were VII on the Mercalli scale. The second was Mw 7.4 La  
238 Crucecita earthquake on June 23, 2020, with the epicenter located about 200 km  
239 southeast of the Pinotepa earthquake (Melgar et al., 2020; Villafuerte et al., 2020),  
240 which produced violent shaking of the maximum intensity of IX and caused widespread  
241 damage. The Grillo network recorded both earthquakes at 15 and 12 stations,  
242 respectively.

243 Using the observations of the Mw 7.2 Pinotepa and Mw 7.4 La Crucecita earthquake,  
244 we test the capability of the Grillo sensor to precisely capture high-amplitude ground  
245 motion accelerations (Fig. 5). We compare the observed peak ground acceleration  
246 (PGA) and the spectral acceleration (SA) with the regional ground motion model (GMM)  
247 of Arroyo *et al.*, 2010. The observed PGA attenuation rate is consistent with the  
248 prediction from the GMM for both earthquakes. The PGA residual mean of  $0.57 \pm 0.36$   
249 suggests a slight but systematic underprediction of PGA by the GMM. The long-period  
250 ground motions represented in SA 3 s attenuate less rapidly than PGA, and the  
251 attenuation rate increases for SA 1.5 s and 0.5 s. The observed SA fit the predicted  
252 attenuation rates well, with almost all observations falling within the two sigma interval  
253 of the GMPE. The residuals suggest that there is no significant period or distance bias  
254 between the observations and the GMM predictions.

255

## 256 **Discussion and Conclusions**

257 This article describes the development of a low-cost MEMS-based seismic instrument  
258 for EEW based on IoT. To test the instrument's performance, we set up a network of 24  
259 instruments on the southwest Pacific coast of Mexico. All data since the deployment in  
260 late 2017 are openly available. We evaluated the sensor performance in terms of data  
261 recovery, self-noise level, dynamic range (DR), and useful resolution (NU). The DR  
262 exceeds 87 and 90 dB for individual components, which corresponds to NU of 15 and  
263 14.5 bits. This ranks the instrument as an ANSS Class B type strong-motion sensor.  
264 The accelerometer can record peak accelerations of a local  $\sim$ M 2.5 earthquake and has  
265 recorded more than 700 earthquakes with clear P-wave onsets. The P-wave peak  
266 ground displacement is a reliable predictor of earthquake magnitude in the entire  
267 magnitude range. The observed values of PGA and SA of 2 major earthquakes are in  
268 good agreement with GMM predictions, showing that the sensor provides reliable  
269 records over a wide range of signal amplitudes. Thus, the Grillo accelerometer meets  
270 the criteria for a reliable, low-cost strong-motion instrument.

271 In August 2020, Grillo launched OpenEEW (<https://openeew.com/>), an open-source  
272 initiative to share data, sensor technology, and detection algorithms, as a Code and  
273 Response with The Linux Foundation project. The OpenEEW enables collaborative  
274 development of the IoT-based EEW system, which focuses primarily on improving the  
275 seismic instrument, seismological algorithms, and development of the cloud platform.  
276 OpenEEW also allows free and unrestricted use of the EEW technology and any

277 archived data, encouraging use of the system in earthquake-prone countries around the  
278 globe.

279 The OpenEEW community has now developed the second generation of the instrument,  
280 the OpenEEW sensor (Fig. 6) that differs from the Grillo sensor described here primarily  
281 in the choice of the CPU. It employs a low-cost, low-power ESP32 microcontroller with a  
282 dual-core Tensilica Xtensa LX6 microprocessor, which reduces the instrument cost and  
283 power consumption. It is contained in a custom-designed PCB board, with integrated  
284 Wi-Fi, Bluetooth, and Ethernet connectivity. Apart from that, it is equipped with RGB led  
285 lights and a buzzer that can be utilized for the EEW warning, and headers enabling the  
286 connection of a GPS module and various other sensors. The instrument works on an  
287 almost plug-and-play basis, with a very straightforward configuration through a  
288 smartphone app that passes the instrument's location and ID to the cloud. Thus, it can  
289 be easily installed and maintained by users with no technical background.

290 The simplicity of the instrument use may enable the general public to contribute to the  
291 EEW system by setting up personal instruments, improving the network density, limiting  
292 the maintenance costs, and securing the EEW sustainability. It may become an efficient  
293 solution for regional and on-site EEW's, or densifying the present networks of traditional  
294 force-balance instruments. A few projects based on OpenEEW are already planned or  
295 underway, such as in Puerto Rico and Nepal. All data collected during these  
296 experiments will be openly available as well.

297

## 298 **Data and Resources**

299 All the data and codes used in this article are openly available. Grillo micro-  
300 electromechanical (MEMS) accelerometer data are available in JSON format at Amazon  
301 S3 storage under the bucket name grillo-openeew  
302 (<https://s3.console.aws.amazon.com/s3/buckets/grillo-openeew>). They can be  
303 downloaded through standard AWS S3 access mechanisms or via OpenEEW Python  
304 packages. The OpenEEW package for Python is available at  
305 <https://github.com/openeew/openeew-python>. OpenEEW sensor can be purchased at  
306 <https://openeew.com>. The ADXL355 sensor specifications can be accessed at  
307 [https://www.analog.com/media/en/technical-documentation/data-](https://www.analog.com/media/en/technical-documentation/data-sheets/adxl354_adxl355.pdf)  
308 [sheets/adxl354\\_adxl355.pdf](https://www.analog.com/media/en/technical-documentation/data-sheets/adxl354_adxl355.pdf). The Servicio Sismológico Nacional (SSN) seismicity  
309 catalog was obtained at <http://www2.ssn.unam.mx:8080/catalogo/>. The observed and  
310 theoretical peak ground acceleration (PGA), spectral acceleration (SA) values were  
311 calculated using MudPy, which can be obtained at [https:// github.com/dmelgarm/mudpy](https://github.com/dmelgarm/mudpy).  
312 All websites were last accessed in November 2020. Some plots were made using the  
313 Generic Mapping Tools version 6 ([generic-mapping-tools.org](http://generic-mapping-tools.org); Wessel et al., 2019).

314

## 315 **Acknowledgments**

316 The development of the instruments was supported by USAID, IBM, Linux Foundation,  
317 Roddenbury Foundation, Arrow Electronics, and Clinton Global Initiative. We thank the  
318 OpenEEW community that contributes to the development of the EEW. We also thank

319 Michael Allman, Allen Husker, and Luis Rodriguez for their help in designing the sensor,  
320 cloud architecture, and deploying the network. SSN data products, station maintenance,  
321 data acquisition and distribution are thanks to its personnel.

322

323 **Competing interests**

324 Authors hold equity in Grillo Inc..

325



326 **References**

327 Allen, R. M., and D. Melgar (2019). Earthquake Early Warning: Advances, Scientific  
328 Challenges, and Societal Needs, *Annu. Rev. Earth Planet. Sci.* **47**, no. 1, 361–  
329 388, doi: 10.1146/annurev-earth-053018-060457.

330 Aranda, J. M. E., A. Jimenez, G. Ibarrola, F. Alcantar, A. Aguilar, M. Inostroza, and S.  
331 Maldonado (1995). Mexico City Seismic Alert System, *Seismological Research*  
332 *Letters* **66**, no. 6, 42–53, doi: 10.1785/gssrl.66.6.42.

333 Arroyo, D., D. García, M. Ordaz, M. A. Mora, and S. K. Singh (2010). Strong ground-  
334 motion relations for Mexican interplate earthquakes, *J Seismol* **14**, no. 4, 769–  
335 785, doi: 10.1007/s10950-010-9200-0.

336 Campillo, M., J. C. Gariel, K. Aki, and F. J. Sánchez-Sesma (1989). Destructive strong  
337 ground motion in Mexico city: Source, path, and site effects during great 1985  
338 Michoacán earthquake, *Bulletin of the Seismological Society of America* **79**, no.  
339 6, 1718–1735.

340 Chen, D., N. Hsiao, and Y. Wu (2015). The Earthworm Based Earthquake Alarm  
341 Reporting System in Taiwan, *Bulletin of the Seismological Society of America*  
342 **105**, no. 2A, 568–579, doi: 10.1785/0120140147.

343 Clinton, J. F., and T. H. Heaton (2002). Potential Advantages of a Strong-motion  
344 Velocity Meter over a Strong-motion Accelerometer, *Seismological Research*  
345 *Letters* **73**, no. 3, 332–342, doi: 10.1785/gssrl.73.3.332.

346 Cochran, E., J. Lawrence, C. Christensen, and A. Chung (2009). A novel strong-motion  
347 seismic network for community participation in earthquake monitoring, *IEEE*  
348 *Instrum. Meas. Mag.* **12**, no. 6, 8–15, doi: 10.1109/MIM.2009.5338255.

349 Cochran, E. S., J. F. Lawrence, C. Christensen, and R. S. Jakka (2009). The Quake-  
350 Catcher Network: Citizen Science Expanding Seismic Horizons, *Seismological*  
351 *Research Letters* **80**, no. 1, 26–30, doi: 10.1785/gssrl.80.1.26.

352 Evans, J., R. Allen, A. Chung, E. Cochran, R. Guy, M. Hellweg, and J. Lawrence (2014).  
353 Performance of Several Low-Cost Accelerometers, *Seismological Research*  
354 *Letters* **85**, 147–158, doi: 10.1785/0220130091.

355 Fleming, K., M. Picozzi, C. Milkereit, the S. and E. working Groups, F. Kühnlenz, the S.  
356 and E. working Groups, B. Lichtblau, the S. and E. working Groups, J. Fischer,  
357 the S. and E. working Groups, *et al.* (2009). The Self-organizing Seismic Early  
358 Warning Information Network (SOSEWIN), *Seismological Research Letters* **80**,  
359 no. 5, 755–771, doi: 10.1785/gssrl.80.5.755.

360 Heimann, S., M. Kriegerowski, M. Isken, S. Cesca, S. Daout, F. Grigoli, C. Juretzek, T.  
361 Megies, N. Nooshiri, A. Steinberg, *et al.* (2017). Pyrocko - An open-source  
362 seismology toolbox and library, doi: 10.5880/GFZ.2.1.2017.001.

363 Holland, A. (2003). Earthquake Data Recorded by the MEMS Accelerometer: Field  
364 Testing in Idaho, *Seismological Research Letters* **74**, no. 1, 20–26, doi:  
365 10.1785/gssrl.74.1.20.

366 Jin, X., Y. Wei, J. Li, H. Zhang, Q. Ma, and L. Kang (2013). Progress of the earthquake  
367 early warning system in Fujian, China, *Earthquake Science* **26**, no. 1, 3–14.

368 Kohler, M. D., E. S. Cochran, D. Given, S. Guiwits, D. Neuhauser, I. Henson, R. Hartog,  
369 P. Bodin, V. Kress, S. Thompson, *et al.* (2018). Earthquake Early Warning  
370 ShakeAlert System: West Coast Wide Production Prototype, *Seismological*  
371 *Research Letters* **89**, no. 1, 99–107, doi: 10.1785/0220170140.

372 Kong, Q., R. M. Allen, L. Schreier, and Y.-W. Kwon (2016). MyShake: A smartphone  
373 seismic network for earthquake early warning and beyond, *Science Advances* **2**,  
374 no. 2, e1501055, doi: 10.1126/sciadv.1501055.

375 Li, H., J. Zhang, and Y. Tang (2017). Testing Earthquake Early Warning Parameters,  
376  $\tau_{pmax}$ ,  $\tau_c$ , and  $P_d$ , for Rapid Magnitude Estimation in the Sichuan, China,  
377 Region Testing Earthquake Early Warning Parameters for Rapid Magnitude  
378 Estimation in the Sichuan Region, *Bulletin of the Seismological Society of*  
379 *America* **107**, no. 3, 1439–1450, doi: 10.1785/0120160386.

380 Li, Y., X. Shan, C. Zhu, X. Qiao, L. Zhao, and C. Qu (2020). Geodetic Model of the 2018  
381 Mw 7.2 Pinotepa, Mexico, Earthquake Inferred from InSAR and GPS Data,  
382 *Bulletin of the Seismological Society of America* **110**, no. 3, 1115–1124, doi:  
383 10.1785/0120190101.

384 Melgar, D., A. Ruiz-Angulo, X. Pérez-Campos, B. W. Crowell, X. Xu, E. Cabral-Cano,  
385 M. R. Brudzinski, and L. Rodriguez-Abreu (n.d.). Energetic Rupture and

386 Tsunamigenesis during the 2020 Mw 7.4 La Crucecita, Mexico Earthquake,  
387 Seismological Research Letters, doi: 10.1785/0220200272.

388 Nof, R. N., A. I. Chung, H. Rademacher, L. Dengler, and R. M. Allen (2019). MEMS  
389 Accelerometer Mini-Array (MAMA): A Low-Cost Implementation for Earthquake  
390 Early Warning Enhancement, *Earthquake Spectra* **35**, no. 1, 21–38, doi:  
391 10.1193/021218EQS036M.

392 USGS Open-File Report 2008-1262: Instrumentation Guidelines for the Advanced  
393 National Seismic System (n.d.): <<https://pubs.usgs.gov/of/2008/1262/>>  
394 (accessed December 4, 2020).

395 Ometepec-Pinotepa Nacional, Mexico Earthquake of 20 March 2012 (Mw 7.5): A  
396 preliminary report | Geofísica Internacional (n.d.): <<https://www.elsevier.es/en-revista-geofisica-internacional-80-articulo-ometepe-pinotepa-nacional-mexico-earthquake-20-S0016716913714715>> (accessed December 4, 2020).

399 Peng, C., Y. Chen, Q. Chen, J. Yang, H. Wang, X. Zhu, Z. Xu, and Y. Zheng (2017). A  
400 new type of tri-axial accelerometers with high dynamic range MEMS for  
401 earthquake early warning, *Computers & Geosciences* **100**, 179–187, doi:  
402 10.1016/j.cageo.2017.01.001.

403 Peng, C., P. Jiang, Q. Chen, Q. Ma, and J. Yang (2019). Performance Evaluation of a  
404 Dense MEMS-Based Seismic Sensor Array Deployed in the Sichuan-Yunnan  
405 Border Region for Earthquake Early Warning, *Micromachines* **10**, no. 11,  
406 735, doi: 10.3390/mi10110735.

407 Peng, C., X. Zhu, J. Yang, B. Xue, and Y. Chen (2013). Development of an integrated  
408 on-site earthquake early warning system and test deployment in Zhaotong,  
409 China, *Computers & Geosciences* **56**, 170–177, doi:  
410 10.1016/j.cageo.2013.03.018.

411 Ryan, W. B. F., S. M. Carbotte, J. O. Coplan, S. O'Hara, A. Melkonian, R. Arko, R. A.  
412 Weissel, V. Ferrini, A. Goodwillie, F. Nitsche, *et al.* (2009). Global Multi-  
413 Resolution Topography synthesis, *Geochem. Geophys. Geosyst.* **10**, Q03014,  
414 doi: 10.1029/2008GC002332.

415 Satriano, C., L. Elia, C. Martino, M. Lancieri, A. Zollo, and G. Iannaccone (2011).  
416 PRESTo, the earthquake early warning system for Southern Italy: Concepts,  
417 capabilities and future perspectives, *Soil Dynamics and Earthquake Engineering*  
418 **31**, no. 2, 137–153, doi: 10.1016/j.soildyn.2010.06.008.

419 Silva, V., D. Amo-Oduro, A. Calderon, J. Dabbeek, V. Despotaki, L. Martins, A. Rao, M.  
420 Simionato, D. Viganò, C. Yepes, *et al.* (2018). Global Earthquake Model (GEM)  
421 Seismic Risk Map (version 2018.1), doi: 10.13117/GEM-GLOBAL-SEISMIC-  
422 RISK-MAP-2018.1.

423 Singh, S. K., E. Mena, and R. Castro (1988). Some aspects of source characteristics of  
424 the 19 September 1985 Michoacan earthquake and ground motion amplification  
425 in and near Mexico City from strong motion data, *Bulletin of the Seismological*  
426 *Society of America* **78**, no. 2, 451–477.

427 Trugman, D. T., M. T. Page, S. E. Minson, and E. S. Cochran (2019). Peak Ground  
428 Displacement Saturates Exactly When Expected: Implications for Earthquake  
429 Early Warning, *J. Geophys. Res. Solid Earth* **124**, no. 5, 4642–4653, doi:  
430 10.1029/2018JB017093.

431 Villafuerte, C., V. M. Cruz-Atienza, J. Tago, D. Solano-Rojas, S. Franco, R. Garza-  
432 Girón, L. A. Dominguez, and V. Kostoglodov (2020). Slow slip events and  
433 megathrust coupling changes reveal the earthquake potential before the 2020  
434 Mw 7.4 Huatulco, Mexico event, preprint, Earth and Space Science Open  
435 Archive: <<http://www.essoar.org/doi/10.1002/essoar.10504796.3>> (accessed  
436 December 4, 2020).

437 Wenzel, F., and J. Zschau (Editors) (2014). *Early Warning for Geological Disasters*,  
438 Springer Berlin Heidelberg, Berlin, Heidelberg, Advanced Technologies in Earth  
439 Sciences, doi: 10.1007/978-3-642-12233-0.

440 Wessel, P., Luis, J. F., Uieda, L., Scharroo, R., Wobbe, F., Smith, W. H. F., & Tian, D.  
441 (2019). The Generic Mapping Tools version 6. *Geochemistry, Geophysics,*  
442 *Geosystems*, 20, 5556–5564. <https://doi.org/10.1029/2019GC008515>

443 Wu, Y.-M. (2015). Progress on Development of an Earthquake Early Warning System  
444 Using Low-Cost Sensors, *Pure Appl. Geophys.* **172**, no. 9, 2343–2351, doi:  
445 10.1007/s00024-014-0933-5.

446 Wu, Y.-M., D.-Y. Chen, T.-L. Lin, C.-Y. Hsieh, T.-L. Chin, W.-Y. Chang, W.-S. Li, and S.-  
447 H. Ker (2013). A High-Density Seismic Network for Earthquake Early Warning in

448 Taiwan Based on Low Cost Sensors, *Seismological Research Letters* **84**, no. 6,  
449 1048–1054, doi: 10.1785/0220130085.

450 Wu, Y.-M., W.-T. Liang, H. Mittal, W.-A. Chao, C.-H. Lin, B.-S. Huang, and C.-M. Lin  
451 (2016). Performance of a Low-Cost Earthquake Early Warning System (P-Alert)  
452 during the 2016 ML 6.4 Meinong (Taiwan) Earthquake, *Seismological Research*  
453 *Letters* **87**, no. 5, 1050–1059, doi: 10.1785/0220160058.

454

455

456 **Full mailing address for each author**

457

458 **Vaclav Kuna**

459 **email: [kunav@ig.cas.cz](mailto:kunav@ig.cas.cz)**

460 Department of Geodynamics

461 The Institute of Geophysics of the Czech Academy of Sciences

462 Boční II/1401

463 Prague, 141 31, Czech Republic

464

465 **Diego Melgar**

466 **email: [dmelgarm@uoregon.edu](mailto:dmelgarm@uoregon.edu)**

467 Earth Sciences Department

468 University of Oregon, Eugene, Oregon, United States

469 100 Cascade Hall

470 1272 University of Oregon

471 Eugene, OR 97403-1272, USA

472

473 **Andres Meira**

474 **email: [andres@grillo.io](mailto:andres@grillo.io)**

475 Tlaxcala 179, interior 201,

476 Hipodromo, Mexico City

477 Mexico 06100



478 **Table 1.** Grillo instrument self-noise RMS, dynamic range (DR), and useful resolution  
 479 (NU), calculated for all 3 sensor components in 3 time periods throughout the  
 480 deployment (see text for details). The values give mean and standard deviation of  
 481 values from individual instruments.

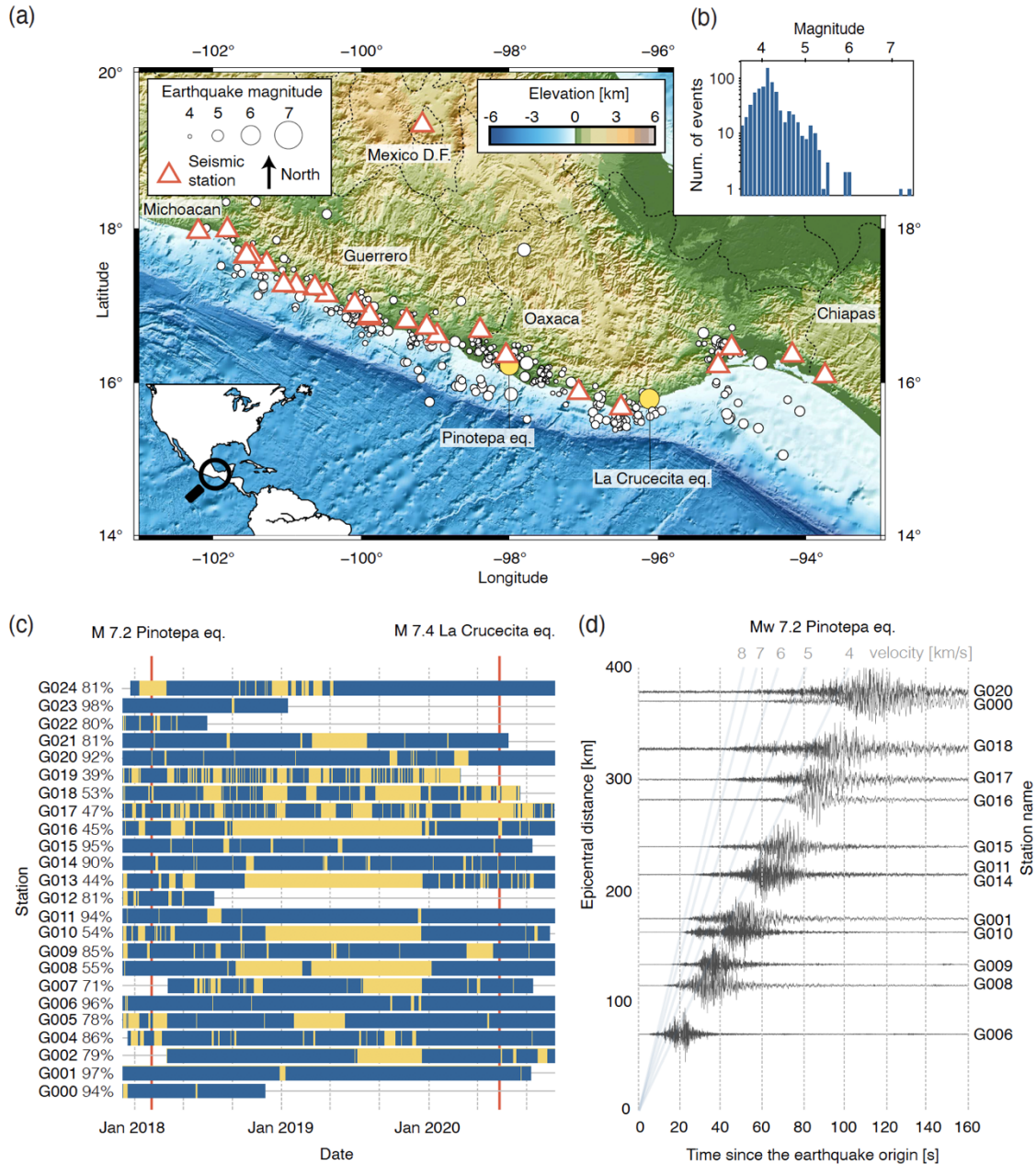
482

**Self-noise (RMS), dynamic range (DR), and useful resolution (NU) of Grillo  
instruments**

Period	Vertical / V			Horizontal 1 / H1			Horizontal 2 / H2		
	RMS	DR	NU	RMS	DR	NU	RMS	DR	NU
1 hour (112500 samples)	[ $\mu\text{g}$ ]	[dB]	[bits]	[ $\mu\text{g}$ ]	[dB]	[bits]	[ $\mu\text{g}$ ]	[dB]	[bits]
June 2018	42.8 $\pm$ 2.0	90.4 $\pm$ 0.4	15.0 $\pm$ 0.1	42.0 $\pm$ 1.3	90.5 $\pm$ 0.3	15.0 $\pm$ 0.0	62.4 $\pm$ 4.1	87.1 $\pm$ 0.6	14.5 $\pm$ 0.1
December 2019	42.9 $\pm$ 2.0	90.4 $\pm$ 0.4	15.0 $\pm$ 0.1	42.0 $\pm$ 1.3	90.6 $\pm$ 0.3	15.0 $\pm$ 0.0	61.6 $\pm$ 2.5	87.2 $\pm$ 0.3	14.5 $\pm$ 0.1
August 2020	42.5 $\pm$ 1.5	90.4 $\pm$ 0.3	15.0 $\pm$ 0.1	41.0 $\pm$ 1.1	90.6 $\pm$ 0.2	15.0 $\pm$ 0.0	61.6 $\pm$ 2.4	87.2 $\pm$ 0.3	14.5 $\pm$ 0.1
<b>Total</b>	<b>42.7 <math>\pm</math> 1.9</b>	<b>90.4 <math>\pm</math> 0.4</b>	<b>15.0 <math>\pm</math> 0.1</b>	<b>42.0 <math>\pm</math> 1.2</b>	<b>90.6 <math>\pm</math> 0.2</b>	<b>15.0 <math>\pm</math> 0.0</b>	<b>61.9 <math>\pm</math> 3.2</b>	<b>87.2 <math>\pm</math> 0.4</b>	<b>14.5 <math>\pm</math> 0.1</b>

483

484



485

486 **Figure 1.** (a) Topographic map of southwest Mexico with locations of Grillo stations and

487 earthquakes recorded by the network (see the main text for details). Epicenters of two

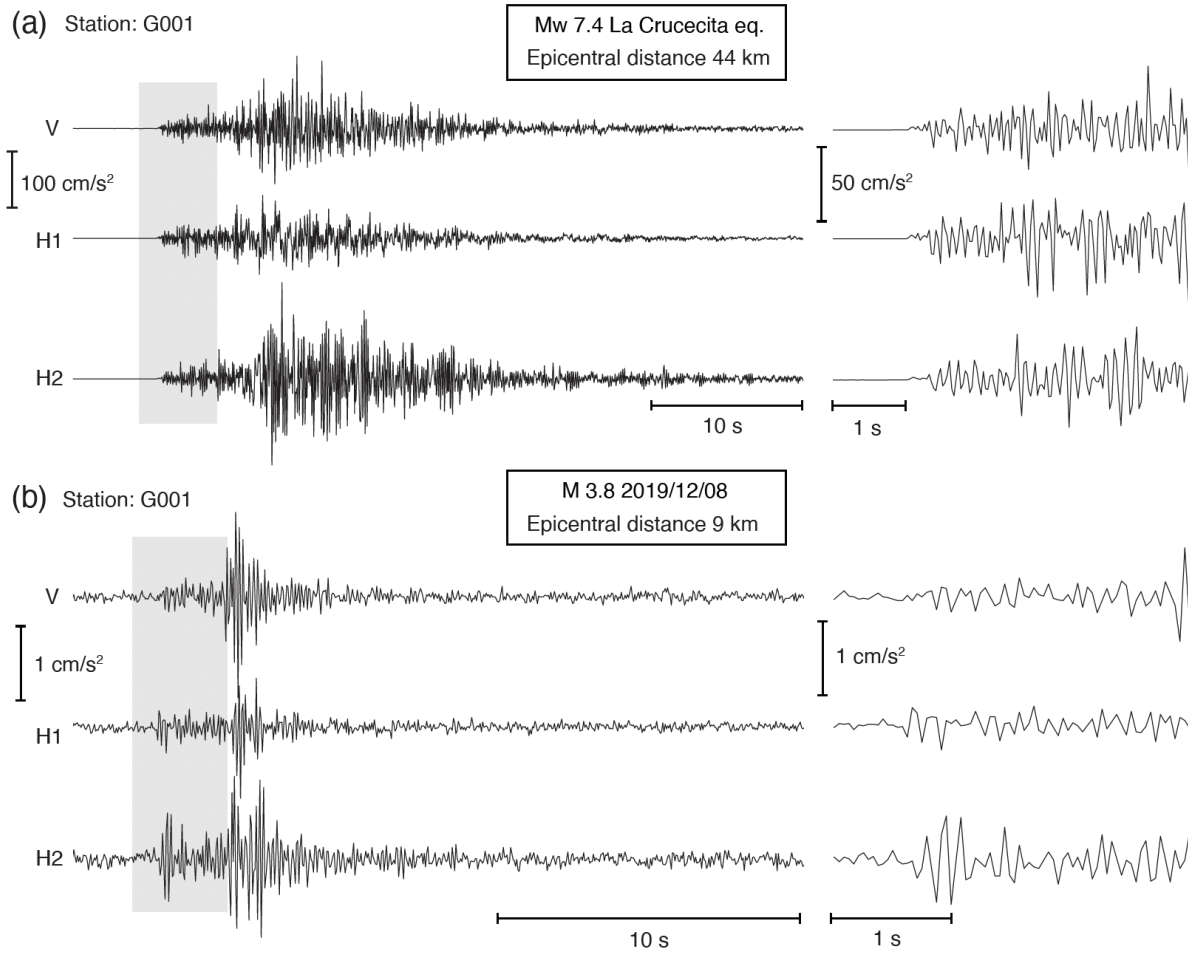
488 major events (2018 Mw 7.2 Pinotepa and 2020 Mw 7.4 La Crucecita) are yellow. We

489 use the GMRT global topographic grid (Ryan *et al.*, 2009). (b) Frequency-magnitude

490 distribution of recorded events. (c) Station data recovery. The plot shows periods of

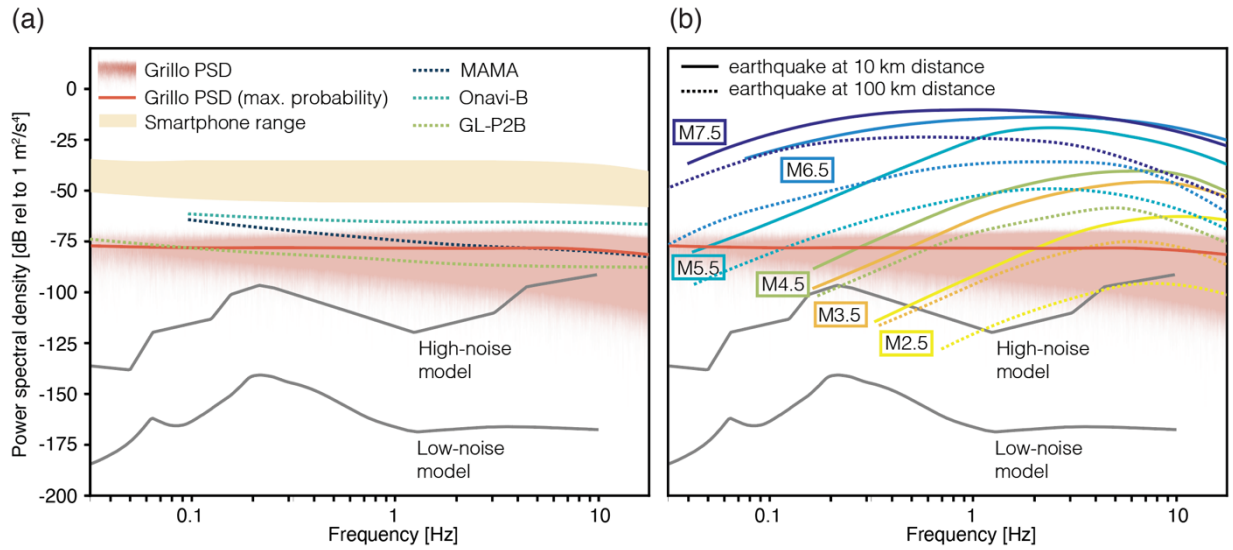
491 continuous data recording (blue) and data gaps (yellow) between November 2017 and  
492 November 2020. The percentage shows the overall recovery rate at each station. Origin  
493 times of two major earthquakes are denoted with red lines. (d) Mw 7.2 Pinotepa  
494 earthquake recorded at the network (displayed up to the epicentral distance of 400 km).

495



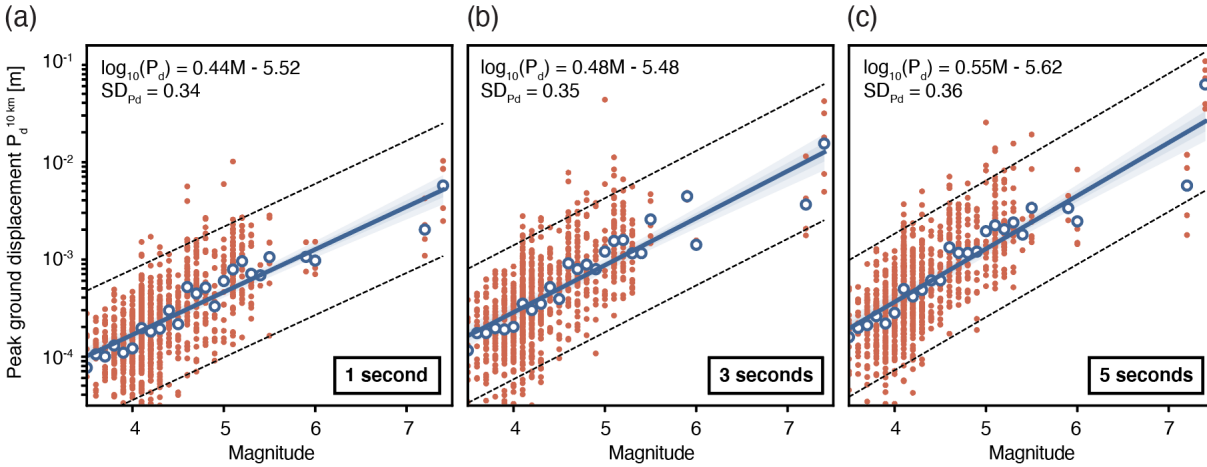
496

497 **Figure 2.** Example waveforms of (a) large (Mw 7.4 La Crucecita) and (b) small (M 3.8  
 498 on 2019/12/08) earthquakes recorded at G001. The left panel shows entire waveforms,  
 499 the earthquake P-waves are amplified on the right.



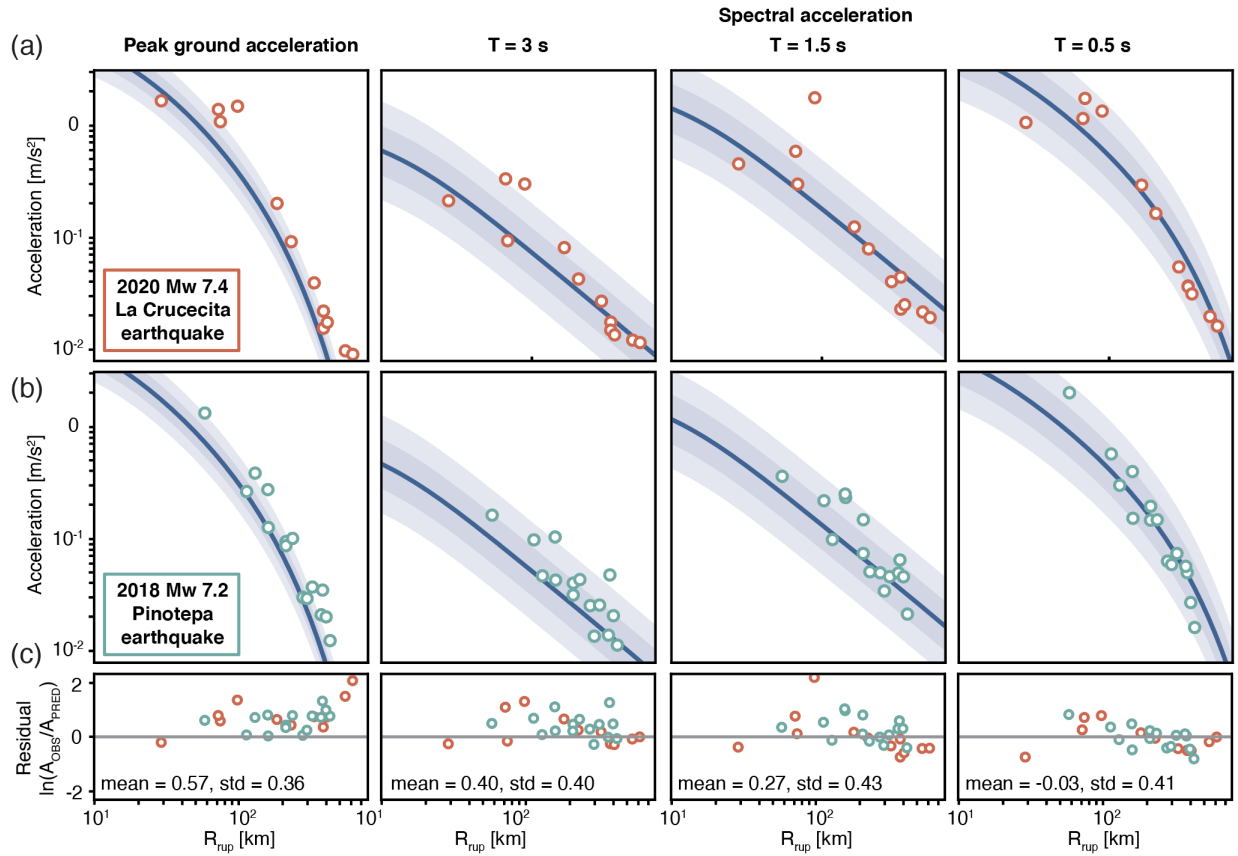
500

501 **Figure 3.** Grillo self-noise power spectral density (PSD) and its comparison with (a)  
 502 other MEMS-based instruments and (b) typical seismic signals. PSD of Grillo sensors  
 503 (light red area) was calculated using vertical components of 1-hour long records from all  
 504 instruments (see text for details). The overall PSD of Grillo instruments (red line) was  
 505 determined as the maximum probability PSD from the probability density function. Grey  
 506 lines indicate low and high microseismic noise levels.



507

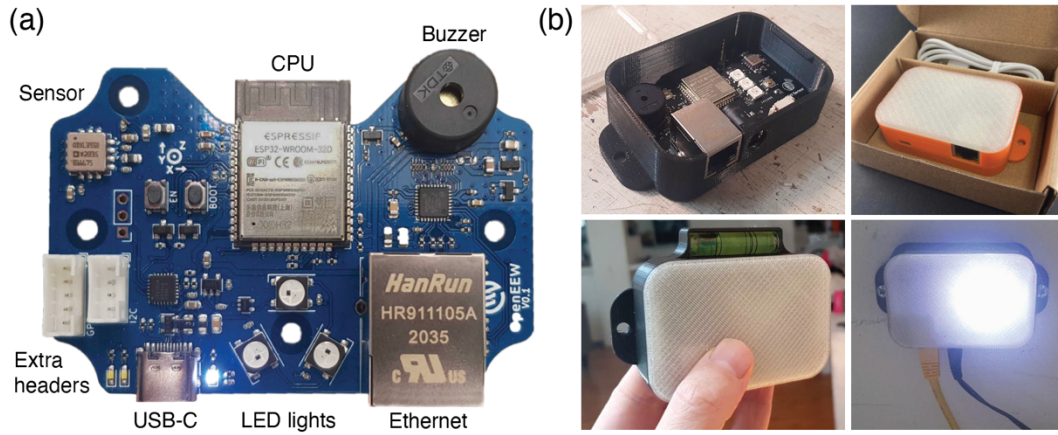
508 **Figure 4.** Peak ground displacement ( $P_d$ ) vs. earthquake magnitude ( $M$ ) using (a) 1 s,  
 509 (b) 3 s, and (c) 5 s segment of initial earthquake P-wave.  $P_d$  is normalized to the  
 510 common epicentral distance of 10 km, assuming the constant  $C$  to be equal to 1. The  
 511  $M$ - $P_d$  relationship is determined by linear regression (blue line) and plotted together with  
 512 the 95% uncertainty interval. Dashed lines represent a 95% interval of residuals ( $P_{d\text{ OBS}}$   
 513  $- P_{d\text{ PRED}}$ ).



514

515 **Figure 5.** Comparison of observed and predicted peak ground accelerations (PGA) and  
 516 spectral accelerations (SA) for (a) 2020 Mw 7.4 La Crucecita and (b) 2018 Mw 7.2  
 517 Pinotepa earthquake. SA is computed for periods of 3, 1.5. and 0.5 s. The predicted  
 518 curves are calculated using GMPE inferred from intermediate and large earthquakes in  
 519 Mexico (Arroyo *et al.*, 2010). 1 and 2 sigma intervals are plotted with shaded blue. (c)  
 520 Residuals of PGA and SA calculated from observed and predicted values as  
 521  $\ln(A_{OBS}/A_{PRED})$ .

522



523

524

525 **Figure 6.** The OpenEEW seismic instrument. (a) The PCB containing all the instrument

526 components. (b) Instrument packaging and deployment.